

A connectivity threshold between grass patches amplifies coastal dune formation

Received: 21 July 2025

Accepted: 24 February 2026

Published online: 19 March 2026

 Check for updates

Paul M. J. Berghuis ^{1,2} ✉, Valérie C. Reijers ³, Johan van de Koppel ^{4,5}, Angeles G. Mayor ⁶, Daniil J. P. Scheifes ², Max Rietkerk ² & Tjisse van der Heide ^{1,5}

Biogeomorphic systems, key providers of ecosystem services, emerge from self-reinforcing feedbacks between landscape-building biota and geomorphic processes. Typically, these feedbacks are considered to operate at an individual patch scale, yet it remains unclear how interactions between patches shape landscapes at larger scales. Here we show how dune-building grasses form functional clusters of interacting patches that strongly amplify engineering capacity. By analyzing a decade of morphological development in an establishing coastal dune system, we discover that dune height is primarily driven by the initial density of neighboring patches, rather than individual patch size. We identify an S-shaped relationship consistent with a spatial percolation threshold: increasing local patch density triggers an abrupt shift from isolated sand-trapping patches to functionally connected clusters that enhance dune growth. This work reveals an important yet overlooked spatial dimension of ecosystem engineering, one that can be harnessed to inform future restoration designs and enhance ecosystem resilience.

Reciprocal organism-landform interactions – so-called biogeomorphic feedbacks – are increasingly recognized as important drivers of landscape formation and ecosystem functioning^{1,2}. Well-known examples of biogeomorphic ecosystems are fluvial landscapes where vegetation controls channel meandering, and peatlands where vegetation retains water and builds landforms by peat accretion^{3,4}. Such systems are particularly common in the coastal zone⁵. Reefs built by corals, mussels, or oysters provide structurally complex hard substrate in sandy environments, filter the water and attenuate hydrodynamics⁶. Similarly, coastal vegetation in mangrove forests, salt marshes, seagrass beds, and coastal dunes attenuates physical flow, leading to the trapping of water- or airborne particles within their canopies and stabilizing sediment through their roots^{7–10}. As these interactions engineer the landscape, they generate important ecosystem services, including coastal defense, carbon storage, freshwater provisioning, and biodiversity sustainment^{11,12}.

An important commonality of all biogeomorphic ecosystems is that the feedbacks between biota and geomorphic processes are self-reinforcing (i.e., positive), meaning that organisms engineer landforms and facilitate each other through local positive density-dependent relationships^{1,5}. For example, mussels, corals, and oysters create hard substrates that promote their own recruitment, while in vegetated systems, plant patches trap and stabilize sediment, enhancing conditions for further plant establishment and growth^{6–8}. Local self-reinforcing feedbacks in combination with a more distant constraint, such as resource limitation or physical stress, have been found to give rise to spatial self-organization^{13,14}. Spatial self-organization is a second commonality of biogeomorphic systems and can be observed in a range of coastal landscapes: mussel beds¹⁵, mangroves⁹, nearshore coral reefs¹⁶, seagrass beds¹⁰, coastal dunes⁸, mudflats¹⁷, and salt marshes⁷.

In many study systems, local self-reinforcing feedbacks lead to spatial self-organization into regular or periodic patterns, i.e., patterns

¹Department of Coastal Systems, Royal Netherlands Institute for Sea Research, Den Burg, The Netherlands. ²Copernicus Institute of Sustainable Development, Utrecht University, Utrecht, The Netherlands. ³Department of Physical Geography, Utrecht University, Utrecht, The Netherlands. ⁴Department of Estuarine and Delta Systems, Royal Netherlands Institute for Sea Research, Yerseke, The Netherlands. ⁵Groningen Institute for Evolutionary Life Sciences, University of Groningen, Groningen, The Netherlands. ⁶Department of Ecology, University of Alicante, Alicante, Spain. ✉e-mail: p.m.j.berghuis@uu.nl

with a characteristic wavelength¹³. However, not all self-organized ecosystems stabilize at a fixed scale. Classic scale-dependent feedback produces stationary bands, spots, or labyrinths whose spacing reflects a balance between short-range facilitation and long-range inhibition, for example in mussel beds¹⁵ or seagrass meadows¹⁰. By contrast, other systems exhibit irregular patches that increase in size over time, as observed in for example coral reefs⁶ and salt marshes¹⁸. Theory suggests that such ‘coarsening’ patterns can arise when long-range inhibition is relatively weak compared with local facilitation, or when inhibition operates at a different scale, for example, by effectively acting as a global constraint^{19–21}. Therefore, understanding why some biogeomorphic systems stabilize while others keep growing hinges on quantifying both the relative strength and spatial extent of inhibitory versus facilitative processes.

In biogeomorphic coastal ecosystems, local self-reinforcing feedbacks are typically suggested to emerge from positive density dependence generated within patches of aggregated individuals^{10,17,22–24}.

However, previous work found that the range of influence of local facilitative effects are not merely restricted to the patch itself, but may extend far beyond¹⁴. In establishing biogeomorphic systems, this spatially extended facilitation could become particularly important when the influence zones of neighboring pioneer patches overlap. In this case, physically separated patches can become functionally connected, for instance, by modulating flow as a collective rather than as individual patches²⁵. Consequently, functional clusters of patches can be formed within the system, whose joint engineering capacity may exceed that of individual patches. We therefore suggest that such a spatially extended effect of local self-reinforcing feedbacks could amplify the landscape-building capacity of ecosystem engineers and represents a thus far overlooked role in the formation of biogeomorphic landscapes.

Coastal dunes are an iconic example of biogeomorphic landscapes. About one third of the world’s coastline consists of sandy shores that are protected by coastal dunes²⁶. Similar to other establishing vegetated biogeomorphic systems (Fig. 1a), developing coastal



Fig. 1 | Patchy coastal systems worldwide and conceptual model of the patch-interaction hypothesis. **a** Global locations of representative coastal biogeomorphic systems characterized by patchy vegetation distributions in the establishment phase. These include dune systems formed by grasses (Netherlands: 52°59'40"N, 4°43'50"E; 2013; USA: 35°13'48"N, 75°32'46"W; 2017; Australia: 34°19'02"S, 115°11'15"E; 2015), salt marshes formed by succulents (China: 31°37'40"N, 121°50'48"E; 2023), mangroves (India: 21°33'54"N, 87°21'36"E; 2024), and seagrass meadows (France: 47°43'02"N, 3°59'00"W; 2019). Insets from Google

Earth (historical imagery dates as indicated): Map data © 2026 Google. Within these systems, patches modulate flows of either wind (dunes) or water (salt marsh, mangrove, seagrass). **b** Conceptual model illustrating sand trapping by isolated dunes through individual flow modulation. **c** Conceptual model demonstrating enhanced sand trapping when dune grass patches occur in closer proximity, enabling functional connectivity by modulating flow collectively. Insets in **(b, c)** show examples of both configurations from drone imagery of the study site.

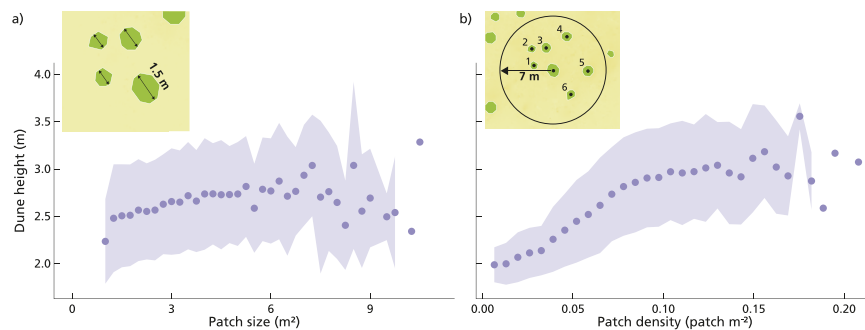


Fig. 2 | Effects of patch size and local patch density on dune height. **a** Average dune height in 2014 as a function of patch size in 2013, with patch sizes binned at 0.25 m² intervals. **b** Average dune height in 2014 as a function of local patch density in 2013 (defined as the number of neighboring patches within a 7 m radius divided by the neighborhood area). Insets illustrate the differences between patch

properties assessed: patch size as proxy for intra patch facilitation (**a**) versus patch density as proxy for inter patch facilitation (**b**). Shaded areas indicate standard deviation; $N_{\text{patches}} = 4349$. For the relationship between patch density and combined neighbor area, see Supplementary Fig. 4 and Fig. 5. Dune height is presented in meters above mean sea level (Amsterdam Ordnance Datum; NAP).

dunes have been proposed to function as self-organizing systems^{8,27}. Coastal dune formation starts with pioneer dune grasses colonizing the beach²⁸. By trapping airborne sediment, these dune grasses become buried, stimulating plants to develop additional shoots and expand, thus further enhancing sand trapping. As a result of this local self-reinforcing feedback, small embryo or nebkha dunes are formed by the individual patches of dune grass^{8,28}. In time, with abundant sediment present, single embryonic dunes will continue to grow, eventually coalescing and maturing to form coastal foredunes^{28,29}. Recent work demonstrated that the spatial organization of shoots within dune grass patches significantly influences sand trapping efficiency and subsequent dune formation at the patch scale^{30,31}. However, at scales beyond individual patches, it remains unclear how spatial interactions among patches influence sand trapping and thus affect the strength and spatial extent of self-reinforcing feedbacks driving dune formation.

Here, we explore how spatially extended interactions among engineering patches, rather than the size of individual patches alone, influence engineering capacity in embryonic (i.e., establishing) coastal dune landscapes. Specifically, we empirically quantify whether the spatial organization of physically separated dune grass patches functionally connects them to amplify dune formation. We hypothesize that, in establishing dunes, collective sand trapping by neighboring patches amplifies early dune formation beyond what individual patches can achieve alone. Following spatial percolation principles³², we expect that when patches lie close enough for their zones of influence to overlap, they form functionally connected clusters whose joint engineering capacity outperforms that of isolated patches. Moreover, we predict that the initial spatial arrangement of patches sets a template for how interactions unfold, making early patch organization a strong predictor of future landscape morphology. In practice, this means that because functional clusters of patches collectively alter air flow^{33,34}, they amplify embryo dune growth by enhancing sand deposition and trapping (Fig. 1c). By contrast, isolated patches do not have that advantage, resulting in slower sand capture and reduced dune growth (Fig. 1b). To test these predictions, we used an extensive dataset of annual high-resolution aerial imagery (0.1 × 0.1 m) spanning over a decade of development in a large (90 ha), establishing dune system. We focused on a 12-ha subsection beyond direct wave impact, where dune development emerged under relatively homogeneous and near-synchronous conditions. Within this subsection, we identified over 4000 dune grass patches and generated detailed elevation maps using photogrammetry, capturing the transition from an embryonic dune field to a mature dune landscape. By linking patch configuration with local morphological change through time, we determine the dominant scale at which ecosystem engineering emerges and assess whether functional connectivity between patches amplifies coastal dune formation.

Results

Between-patch interactions amplify dune formation

Our results support the hypothesis that dune height development is not primarily driven by within-patch facilitation, indicated by the size of a patch, but instead arises from interactions between neighboring patches that jointly amplify dune growth. As a first step, we tested whether initial patch size correlates with dune height one year later, but no clear relationship was found (Fig. 2a; Spearman's $\rho = 0.18$, $p < 0.001$). We then examined how the local density of neighboring patches influences dune height (within a 7 m radius of each focal patch, see “Methods” and Supplementary Fig. 1). The results revealed that dune height much better predicted by local patch density (Fig. 2b; Spearman's $\rho = 0.57$, $p < 0.001$). Similar relationships can be found for Δ dune height (Supplementary Fig. 2). Finally, we checked whether local patch density could be a product of underlying environmental factors such as initial topography or distance to the shoreline within our study area. Although initial topography shows a significant correlation, neither is a strong driver of patch density (Spearman's $\rho = 0.097$, $p < 0.001$ and $\rho = 0.019$, $p = 0.199$ respectively) or future dune height (Supplementary Table 1 and Fig. 3). These findings show that dune formation is not an isolated outcome of individual patch performance, but rather an emergent property of spatially clustered patches. This implies that by building a shared dune body, physically separated patches become functionally connected.

Between-patch interactions create a template for long-term dune landscape formation

Long-term analyses of dune landscape development highlight that between-patch interactions not only shape dune height in the short term (Fig. 2b) but also have a lasting effect as the system continues to develop over multiple years (Fig. 3a). Specifically, we found that the initial patch density in 2013 has an evident positive effect on dune height for 8 consecutive years from the period 2014–2023 (Fig. 3a). Indeed, for all years, dune height follows an S-shaped curve as function of initial patch density, with limited dune growth for a patch density of below 0.03 patch m⁻², a steep increase around 0.05 patch m⁻², after which it flattens off from 0.10 patch m⁻². This S-shaped relationship can be best described by a Hill function (see Eq. (2) in the “method” section and Supplementary Table 2 for model fitting). This long-term, nonlinear response shows how early patch density leaves a lasting imprint on landscape development, with dune growth accelerating once a critical density threshold is surpassed.

The effect of initial patch density on dune height becomes increasingly nonlinear over time, yielding a sharper more threshold-like transition in early patch density beyond which dunes rapidly build up. This is reflected in the increasing sigmoidicity exponent h of the S-shaped curves (Fig. 3b). The combined height of the system builds up

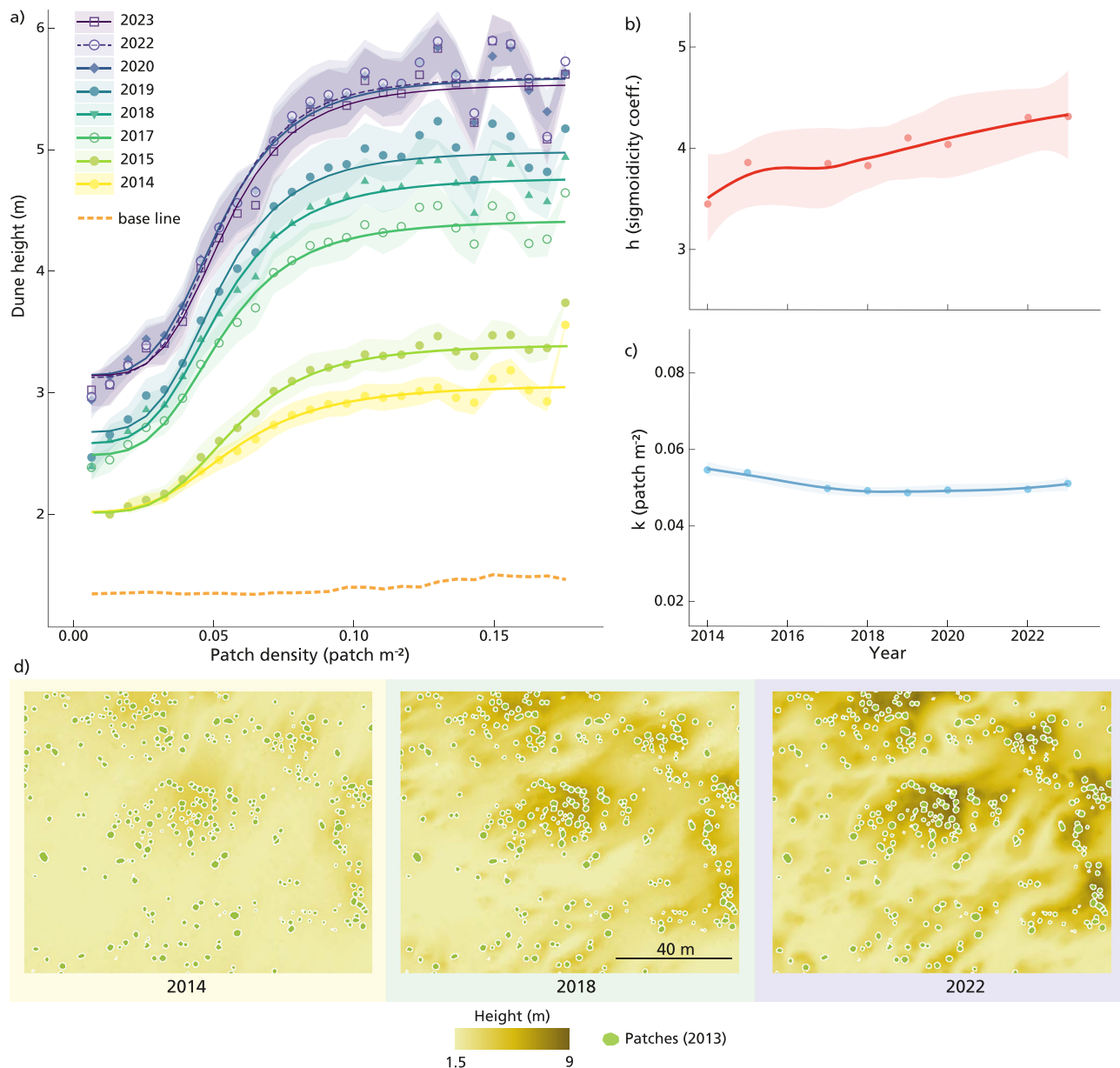


Fig. 3 | Long-term dune development as a function of local patch density.

a Average dune height (2014–2023) as a function of local patch density in 2013. Curves follow the Hill equation of Eq. (2). Shaded areas indicate standard deviation (scaled to 0.2 of actual value for clarity; full standard deviations are shown in Supplementary Fig. 6); $N_{\text{patches}} = 4349$. The orange dashed line indicates the base line topography prior to vegetation establishment (2010; see Supplementary Fig. 7). **b**, **c** Hill-curve parameters h (sigmoidicity, controlling curve shape) and k

(inflection point, indicating maximum slope) over time (2014–2023), derived from the fits shown in panel (a). Curves are fitted using LOESS smoothing; shaded areas indicate confidence intervals. **d** Example area from the study system, showing vegetation patches (green) in 2013 and subsequent dune development in 2014, 2018, and 2022 based on digital elevation models (DEMs). Dune height is presented in meters above mean sea level (NAP).

relatively rapid at first and stabilizes in the final years of the analysis, as indicated by the spacing between the S-curves (Fig. 3a; see for long term dune development Supplementary Fig. 7). Interestingly, the inflection point k stays relatively constant over time (0.054 ± 0.003 patch m^{-2} ; Fig. 3c). Together, these analyses indicate that dune formation is governed by an initial patch-density threshold whose influence intensifies over time.

It is striking that the spatial distribution of vegetation patches in the earliest year (2013) best predicts dune height up to a decade later. In support of previous analyses, the explanatory power of patch density on dune height declines as dune grass patches of this initial embryonic system grow and expand over time (see for the effect of patch density from 2017 and 2021 Supplementary Fig. 8 and Table 3).

This further highlights that it is predominantly the initial patch distribution and the associated patch densities that shape future dune development. The strength of this early effect can also be visually recognized by comparing the 2013 vegetation map with elevation change over time (Fig. 3d). Together, these results highlight that it is the initial organization of vegetation, rather than its later expansion, that sets the development trajectory of dune growth.

A connectivity-based threshold drives nonlinear dune growth

The threshold-like relationship between patch density and dune growth observed in Fig. 3a shows a striking parallel with the percolation threshold that is well known from statistical physics³². In our case, the inflection point k of the S-shaped relationship (Fig. 3a) marks the

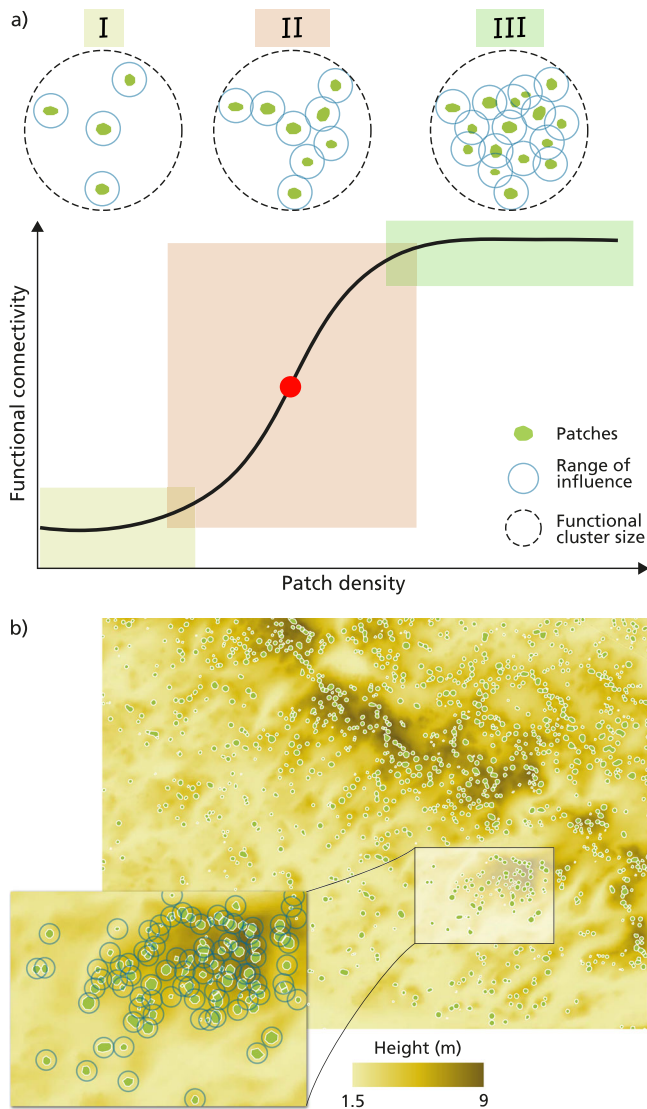


Fig. 4 | Conceptual model illustrating how vegetation patch density controls functional connectivity and leads to a percolation-like transition. a At low densities (yellow; I), isolated vegetation patches have minimal sand-trapping effectiveness. Increasing density (red; II, the percolation zone) causes patches to become functionally connected, enhancing sand trapping. Beyond a critical threshold (green; III), further increases in density yield diminishing returns due to saturation of connectivity. This transition is represented by a sigmoidal curve, with a critical density threshold (red dot) marking the center of the percolation zone, i.e., the patch density at which the spanning probability equals 0.5. The blue circle indicates a patch's suggested range of influence; the dashed circle indicates the functional cluster size. **b** Example visualization of vegetation patches (from 2013) projected onto dune elevation data (2023), highlighting ranges of influence (blue). The inset demonstrates how overlapping influence zones result in a collective dune body of amplified height.

patch density around which small changes lead to disproportionately large deviations in dune height, a hallmark sign of systems undergoing a connectivity-driven transition³⁵. Indeed, interpreting the inflection point k of the S-shaped relationship as a percolation-like threshold suggests that, around this density, a critical transition occurs: patches become functionally connected forming large “spanning” clusters (Fig. 4a). Below the percolation zone around k , patch densities are too low to form such clusters. Above the percolation zone, the system is “percolated”—i.e., functional clusters have formed—implying that from that point onward additional patches will yield diminishing returns due to saturation of connectivity (Fig. 4a). Assuming each patch affects its

surroundings within a circular range of influence, using continuum (disk) percolation³⁶, we can calculate the minimal radius of this range of influence required to form a spanning cluster at the patch density of k (Fig. 3a $k \approx 0.05$ patch m^{-2} ; see “Methods” for details). This yields a range of influence with a 2.27 m radius and a maximum interaction distance between patches of 4.54 m (to connect their ranges of influence). Figure 4b illustrates how this estimated 2.27 m allows the range of influence of patches to overlap, forming a functionally connected cluster that uses its joint engineering capacity to build a single dune body. Thus, applying the percolation framework on our empirical data exposes a mechanistic understanding of the scale at which individual patches engineer their environment and how connectivity between patches amplifies this process to shape the entire dune landscape.

To test whether the nonlinearity in Fig. 3a indeed reflects a connectivity mechanism, we performed three complementary analyses. First, we tested whether the maximum interaction distance predicted by percolation theory (4.54 m) appears independently in our data. When relating mean nearest-neighbor distance to dune height, we find an S-shaped relation for which amplified dune growth happens within a given distance (4.12, 4.48 and 5.11 m; Fig. 5d bc). These distances closely match the 4.54 m maximum interaction distance. Second, using that same maximum interaction distance, we quantified “spanning”-cluster formation as a function of patch density (Fig. 5d). Indeed, the results yield the expected sigmoidal increase. The fraction of patches being part of large clusters rises most steeply near the inflection point k and saturates where the dune-height curves level off (Fig. 3a). Third, because our inflection point k is estimated within a finite window (the local neighborhood), we examined how k shifts with window size (L) (Supplementary Fig. 10). In the case k represents a connectivity threshold, percolation theory predicts a characteristic scaling for k : larger windows require less density to connect (more alternative paths), so $k(L)$ decreases and converges. For two-dimensional percolation, $k(L)$ yields a linear relation with $L^{-0.75}$ (see Eq. (6))³². Consistent with this, Fig. 5e shows that k systematically decreases with window size and then stabilizes, thereby it obeys the hallmark $L^{-0.75}$ scaling for a connectivity threshold (Fig. 5f). Importantly, two alternative explanations would show a very different scaling trend: (i) if the spatial patch distribution alone (short-range clustering; see Supplementary Fig. 9) was responsible, k logically should increase and then plateau with window size; and (ii) if dune height depended only on total cover (no connectivity), the threshold would stay constant across window sizes. Together, these tests show that once patches are close enough to interact, functional connectivity emerges and dune growth accelerates, consistent with a connectivity-based threshold.

Discussion

Our work demonstrates that ecosystem engineering, typical of biogeomorphic systems, can extend beyond the scale of individual patches and arise from functionally connected neighbors. Specifically, we found that in establishing coastal dune systems, spatially separated neighboring patches interact to amplify sand trapping and thus dune growth compared to single, isolated patches. Such facilitative interactions are governed by a connectivity (percolation-like) threshold: when patches lie in close enough proximity to form functional clusters, dune growth increases nonlinearly, yielding a S-shaped relationship between patch density and dune height. Moreover, differences in dune height between clusters and isolated patches increase over time, since clustered vegetation accelerates dune growth relative to more isolated configurations. As a result, the initial spatial organization of vegetation patches acts as a functional template for long-term morphological development, linking early patch densities to future landscape-scale outcomes.

Concepts from percolation theory highlight the role of connectivity in the S-shaped relation between dune height and patch density. For percolation in its classical, structural form (site/bond

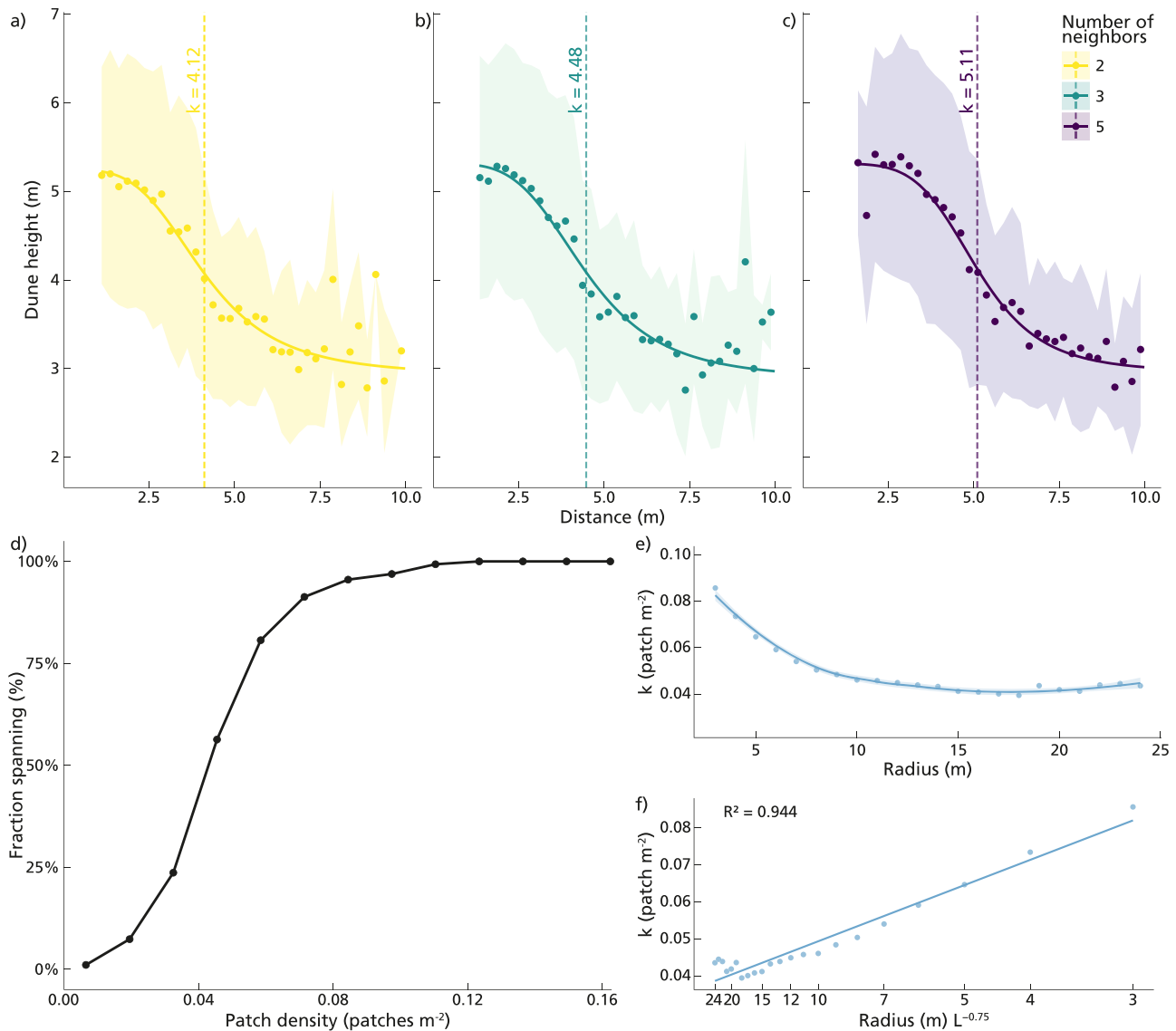


Fig. 5 | Empirical support for the conceptual model in Fig. 4. **a–c** Dune height (2023) as a function of nearest-neighbor distance (2013), averaged over the 2, 3, and 5 nearest neighbors. Trend lines show Hill-function fits (Eq. (1)), where k represents the distance threshold (vertical dashed lines). These thresholds closely match the maximum interaction distance predicted from percolation theory (~4.54 m). Shaded bands show the standard deviation. **d** Using this interaction distance, we calculated the fraction of patches in “spanning” clusters (%) as a function of local patch

density. The spanning fraction increases most steeply near the inflection point k from Fig. 3c (0.054 ± 0.003 patches m^{-2}) and saturates where dune-height curves level off. **e** Dependence of k on window radius: k decreases with increasing radius and then approaches a window-independent limit. **f** Finite-size scaling test: plotting $k(L)$ against $L^{-0.75}$ (x -axis, labeled by the corresponding radii in meters) indeed yields an approximately linear relationship ($R^2 = 0.94$).

percolation on lattices)³², connectivity emerges abruptly once occupancy crosses the percolation threshold, typical examples are fluid conduction through porous media³⁷ and electric conductivity³⁸. However, our study system more closely follows the principles of continuum (disk) percolation³⁶, where it is not the entities themselves but their ranges of influence that overlap to form functionally connected clusters, e.g., habitat connectivity³⁹. Importantly, our study system is spatially heterogeneous and noisy: e.g., variation in patch size and geometry, non-random clustering, and stochastic disturbances broaden an idealized system scale transition into a percolation zone, blurring an exact percolation threshold but preserving an overall sigmoidal response. Our finite-size scaling of k and the nearest-neighbor distance test indicate that this noise does not erase the underlying mechanism. Instead, once local ranges of influence overlap sufficiently, this functional connectivity accelerates dune building. Beyond this point, adding even more patches yields diminishing returns as functional clusters already have been formed.

Coupling biogeomorphic feedbacks with the percolation framework, offers an explanation of why the initial spatial arrangement of dune-grass patches is such a strong predictor of future dune height. It is the percolation-like transition of dune-grass patches into functional clusters that sets the stage for future dune development, after which nonlinear plant–sediment feedbacks (Fig. 1b) shape the observed S-curves to become steeper over time (Fig. 3a). The relatively constant k across years (Fig. 3c) is consistent with a structural connectivity threshold, while the increasing h (Fig. 3b) likely reflects strengthening dynamic feedbacks. The timing and position of functional cluster formation are context dependent, affected by a site-specific range of influence, which likely varies with sediment size and supply, wind regime, and species traits^{28,29}. Similar condition dependence has been observed for other biogeomorphic systems; for instance, in salt marshes, the spacing and size of gullies depend strongly on hydrodynamic forcing^{22,40}. More broadly, our findings align with previous work highlighting the importance of early spatial arrangements in

biogeomorphic systems, whether shaped by pioneer life histories⁴¹, recruitment strategies⁴², or vegetation presence in general⁷.

Our results have important implications for the conservation and restoration of coastal dunes and biogeomorphic systems in general. Coastal biogeomorphic systems are notoriously difficult and often prohibitively expensive to restore^{43,44}. While growing evidence suggests that naturally emerging spatial patterns can be harnessed to improve restoration outcomes^{15,45}, most current efforts still rely on evenly spaced planting designs, such as uniform grids of Marram grass (*C. arenaria*) seedlings, that bear little resemblance with the patchy organization that develops naturally (Fig. 1a). Recent studies demonstrate that clumped planting in high density patches can maximize local facilitation and substantially improve restoration success^{22–24,31,34,46}. Our findings suggest that this principle goes beyond just patch size: not only should plants be grouped in patches, but these patches should be arranged such that they can interact similar to what is observed in natural systems. For our specific dune system, the maximum interaction distance lies around 4.5 m, to allow for efficient percolation into functional clusters that in turn amplify dune development and thus landscape formation. Such an interpatch distance deviates from patch configurations used in state of the art restoration experiments^{46–48}, where in general higher dune grass densities are applied. Therefore, incorporating interpatch facilitation into restoration design could not only enhance ecosystem recovery, but result in much more cost-effective designs as well^{49,50}.

Coastal biogeomorphic systems are under increasing pressure and are degrading at an alarming rate⁵¹, yet their capacity for self-recovery depends on the very facilitative interactions that build

them⁴⁹. Our study reveals an overlooked scale of ecosystem engineering capacity, showing that physically separated vegetation patches can percolate into highly efficient, landscape-engineering clusters. In doing so, we expose a new level of self-organization in coastal dunes; from behavioral processes within individual plants³¹, to between-patch functional connectivity. Ecological resilience theory predicts that ecosystems best withstand disturbance when positive feedbacks operate at multiple scales⁵². Indeed, work from mussel beds has linked multi-scale self-organization to enhanced resilience of biogeomorphic systems^{15,53}. Our findings support the notion that multi-scale self-organization can be critical for maintaining ecosystem resilience and highlight that these processes are also vital in the establishment phase of biogeomorphic landscapes.

Methods

Study site

To test our hypothesis, we required a naturally formed embryonic dune field that recently transitioned into a mature landscape. Since our study investigates landscape-building processes, an ideal location would experience minimal limitations in accommodation space, sediment availability, and seasonal erosion^{54–56}. Additionally, for this dune system high-resolution aerial imagery capturing the main development of the system needed to be available. The Hors on Texel, the Netherlands (52°59'43.1"N 4°43'46.0"E, Fig. 6), turned out to be a very suitable location. The Hors consists of an unmanaged, actively developing dune system (~90 ha in 2024), progressing south-westward over recent decades. Flood erosion at the Hors is minimized by an extensive beach plain fronting the embryonic dunes, which attenuates wave

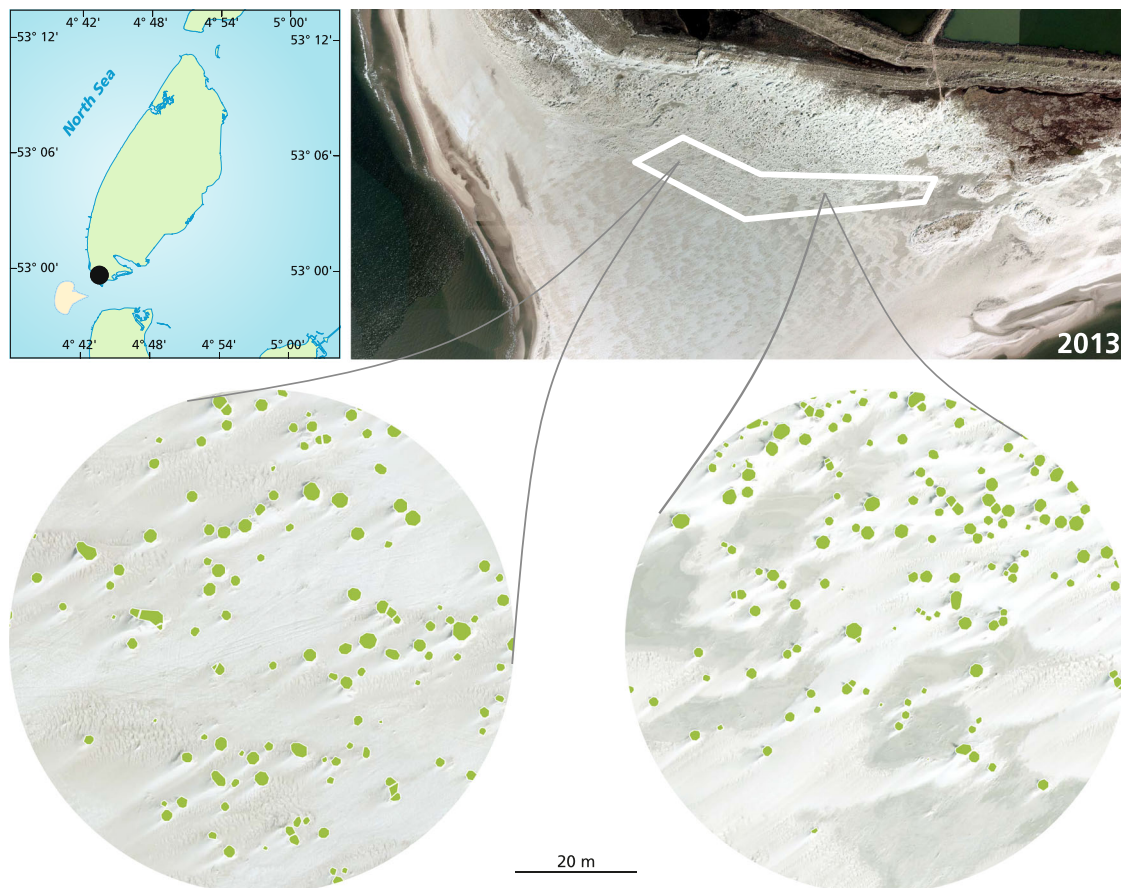


Fig. 6 | Location of the study site along the North Sea coast (52°59'43.1"N 4°43'46.0"E). The site, covering ~90 ha, is situated on the southern tip of Texel, one of the barrier islands in the northern Netherlands. The white box indicates the location of our study site (~12 ha) oriented parallel to the shoreline, along the sea-to-

land gradient. From this site two representative sections are highlighted showing the detected dune grass patches (in green) on top of the corresponding aerial image of 2013 (adapted from beeldmateriaal.nl).

impact^{57,58}. This beach plain also provides sufficient accommodation space for dune expansion and serves as a large fetch area for wind-driven sediment transport^{56,59}. Wind directions vary throughout the year, with South-Western winds being most common (Supplementary Fig. 11). For our analysis, we focused on a 12-ha subsection of the Hors, representing an embryonic dune field establishing around 2011–2012, with clearly identifiable dune grass patches and embryo dunes in the imagery from 2013 onward (Fig. 6). This subsection is oriented parallel to the tideline and was part of a significant colonization event. By 2013, pioneer grasses had formed distinct embryonic dunes, with minimal spatial or temporal gradients, ensuring uniform age and environmental conditions across the area. At that time, dune grass patches covered 8.5% of this area, comprising 4,349 embryo dunes with an average patch size of 2.3 m². Two species dominate dune formation here: *Elytrigia juncea* (Sand couch) and *Calamagrostis arenaria* (formerly *Ammophila arenaria*, Marram grass)⁶⁰. *E. juncea* acts as the pioneer species, facilitating landscape modification and subsequent colonization by *C. arenaria*, which is the superior dune builder⁶¹. Although *E. juncea* likely initiated landscape changes at the study site, the distinct embryo dunes visible from 2013 onwards were predominantly formed by *C. arenaria*.

Data

Aerial imagery of the Hors was provided by the municipality of Texel and Beeldmateriaal, both of which conduct annual high-resolution airborne surveys. We used pre-processed orthomosaics from the national airborne survey (0.1 × 0.1 m), to detect and extract dune grass patches (Beeldmateriaal 2010–2021; Beeldmateriaal HRL 2021–2023, CC BY 4.0). Digital elevation models (DEMs) were generated from stereo photos provided by the municipality of Texel using Agisoft Metashape, covering the years 2014, 2015, 2017–2020, and 2022–2023, with horizontal resolutions ranging from 0.05 to 0.07 m. All imagery was captured in early spring, prior to the main growing season (February–April). To evaluate the beach topography prior to our main study period (2008–2013), we used preprocessed elevation data from Hoogtebestand Kust (5 × 5 m). We extracted dune grass patches using a geospatial deep learning platform (Picterra). A custom model combining object detection and feature masking enabled us to delineate both the location and spatial extent (surface area and perimeter) of individual patches (see for examples feature masking Fig. 6, and for more details on model approach: www.picterra.ch).

Data analysis

Between-patch interactions amplify dune formation. We first examined the relationship between the size of dune grass patches in the initial embryonic dune field (2013) and their corresponding dune height in the subsequent year. For each patch, dune height was extracted from all available DEMs using its centroid coordinates. Next, we tested whether local patch density could explain future dune height. Local patch density was calculated by counting the number of neighboring patches within a circular search radius (r_{search}) around each patch center, assuming isotropic interactions for simplicity.

To determine an ecologically relevant neighborhood radius, we related dune height to neighbor counts for radii from 2 to 30 m using Spearman's rank correlation coefficient (ρ) and applied the elbow criterion for scale-dependent patterns⁶². The elbow location was identified with piecewise (broken-stick) regression (segmented package in R)⁶³ as the smallest radius at which $\geq 95\%$ of the maximum ρ was reached, and further increases in radius yielded only marginal gains in explanatory power. This procedure identified 7 m as the neighborhood radius (see Supplementary Fig. 1), which we used in all subsequent analyses. A patch was considered a neighbor if its centroid lay within this radius (r_{search}). Local patch density was defined as:

$$\text{Patch density} = \frac{N_{\text{patches}}}{(\pi r_{\text{search}}^2)} \quad (1)$$

Underlying environmental factors. To test whether the observed relationship between patch density and dune height reflects underlying environmental gradients, we quantified distance to shoreline and initial elevation and evaluated their associations with local patch density and future dune height. We computed distance to the shoreline as the planar distance from each patch centroid to the mapped shoreline for the year 2013; initial topography was extracted at each patch centroid from the DEM of the year 2010 (in this year vegetation cover was neglectable, see Supplementary Fig. 7). For the correlation between initial topography, distance to shoreline and patch density we used Spearman's rank correlation. Moreover, for the relation of these variables to future dune height, we used a standardized multiple linear model with future dune height as the response and patch density, distance to shoreline, initial topography, and patch size as predictors (see for details Supplementary Table 1 and Supplementary Fig. 3). To support these tests, Supplementary Fig. 7 presents aerial imagery of system development from a bare beach to a mature dune field (2008–2023), together with time series of total dune volume and vegetation cover, illustrating the onset of dune formation following vegetation establishment.

Between-patch interactions create a template for long-term dune landscape formation. To determine the best functional fit between patch density and future dune height, we tested multiple candidate models: linear, power-law, negative exponential, and a generalized Hill function⁶⁴. Based on the Akaike Information Criterion (AIC), the Hill function consistently provided the best fit across all elevation years (see Supplementary Table 2 for model fitting details). The generalized Hill function can be defined as:

$$y = y_{\min} + \frac{(y_{\max} - y_{\min})x^h}{k^h + x^h} \quad (2)$$

Within the context of this study, the parameters of Eq. 2, can be best described as follows. Dune height (m) is represented by y . With y_{\min} being the minimum dune height predicted at very low patch densities, indicating the baseline dune growth by isolated patches. y_{\max} stands for the maximum dune height achievable as patch density increases. k is the inflection point of the curve, marking a key threshold in the relationship between patch density and dune development at the steepest point of the curve. The Hill coefficient h , controls the steepness, or sigmoidicity, of the curve around k . A higher value of h indicates a sharper, more threshold-like transition in dune growth.

A connectivity-based threshold drives nonlinear dune growth. To test whether the observed nonlinearity between patch density and dune height reflects a connectivity mechanism, we interpreted the inflection point k of the Hill function (Eq. 2) as the midpoint of a percolation transition. We then translated k into an interaction length by calculating the range of influence around each patch centroid needed to form a spanning cluster at the observed patch density for k . We treated each vegetation patch as the center of a disc of influence with radius r , such that two patches interact when their disks just touch. The expected number of neighbors within distance r of a focal patch is:

$$N(r) = \rho \pi r^2 G(r) \quad (3)$$

Where ρ is patch density (patches m⁻²), πr^2 is the area of the neighborhood, and $G(r)$ is the pair-correlation function describing the degree of clustering relative to a random spatial distribution (estimated from a pair-correlation function of the system; Supplementary Fig. 9). Following continuum disk percolation for a two-dimensional system, a spanning cluster appears when a patch is directly connected to, on average, $\lambda_c \approx 1.128$ neighbors³⁶. At the

percolation point we therefore require:

$$N(r) = \lambda_c = 1.128 \quad (4)$$

Combining Eq. 3 and eq. 4 gives:

$$r = \sqrt{\frac{\lambda_c}{k\pi G(r)}} \quad (5)$$

Since $G(r)$ is based on r , a few iterations have to be calculated to find r that fits with the clustered spatial distribution of the system. We then defined the maximum interaction distance between patch centroids as $d_{\max} = 2r$.

Using d_{\max} , we performed three complementary analysis. First, we related dune height to the mean nearest-neighbor distance per patch (averaged over the 2, 3, and 5 closest neighbors; centroid-to-centroid). We fitted Hill functions (Eq. 2) to these relations to estimate distance thresholds. For this, we used the value of the inflection point k , which we later compared to the theoretically derived d_{\max} . Second, we treated patches as connected when their centroids were $\leq d_{\max}$ apart and identified connected sets of patches. We classified a set as “spanning” when it bridged a distance needed to connect opposite sides of our 7 m radius neighborhood window. We then quantified, across patch density, the fraction of patches belonging to such spanning components.

Third, we performed a finite-size scaling analysis to test whether the density threshold k behaves as expected for a 2-D percolation transition. We re-estimated k for different window sizes (L) with radii (3–24 m; see Supplementary Fig. S10) as the inflection point of the patch density versus dune height curves, computing local patch density as in Eq. (1). In finite systems the apparent percolation threshold depends on the window size (L), interpreting k as the percolation threshold, finite-size scaling theory predicts:

$$k(L) = k_c + aL^{-\frac{1}{\nu}} \quad (6)$$

Where k_c is the density threshold in an infinite system, a is a constant, and ν is the correlation-length exponent. The universal value for ν in 2D percolation³² is $\nu = 4/3$, so $k(L)$ should vary approximately linearly with $L^{-0.75}$. Therefore, to test whether the observed finite-size dependence of our patch density versus dune-height threshold is consistent with 2-D percolation, we regressed $k(L)$ against $L^{-0.75}$. Unless noted otherwise, analyses above included all patches present in 2013 ($N_{\text{patches}} = 4349$ patches). All analyses described here were performed in R (v2024.04.2).

Data availability

Links to publicly available aerial imagery and elevation maps, the shapefile of the study area and shapefiles of the extracted dune grass patches that support the main findings of this study are available in DataverseNL at (<https://doi.org/10.34894/IDHH59>). In addition, the source data of the main text figures are provided as a Source Data file. Source data are provided with this paper.

Code availability

All code (developed in R) used to calculate the patch metrics can be accessed through DataverseNL at (<https://doi.org/10.34894/IDHH59>).

References

- Murray, A. B., Knaapen, M. A. F., Tal, M., & Kirwan, M. L. Biomorphodynamics: physical-biological feedbacks that shape landscapes. *Water Resour. Res.* **44**, W11301 (2008).
- Larsen, A., Nardin, W., Van de Lageweg, W. I. & Bätz, N. Biogeomorphology, quo vadis? on processes, time, and space in biogeomorphology. *Earth Surf. Process. Landf.* **46**, 12–23 (2021).
- Finotello, A. et al. Vegetation enhances curvature-driven dynamics in meandering rivers. *Nat. Commun.* **15**, 2024 (1968).
- Tempink, R. J. et al. Recovering wetland biogeomorphic feedbacks to restore the world’s biotic carbon hotspots. *Science* **376**, eabn1479 (2022).
- Corenblit, D. et al. Engineer pioneer plants respond to and affect geomorphic constraints similarly along water–terrestrial interfaces world-wide. *Glob. Ecol. Biogeogr.* **24**, 1363–1376 (2015).
- Purkis, S. J., Van De Koppel, J., & Burgess, P. M. Spatial self-organization in carbonate depositional environments. In: *Autogenic Dynamics and Self-Organization in Sedimentary Systems*. pp. 53–66 (2016).
- Van de Vijssel, R. C. et al. Vegetation controls on channel network complexity in coastal wetlands. *Nat. Commun.* **14**, 7158 (2023).
- Bonte, D. et al. Biomorphogenic feedbacks and the spatial organization of a dominant grass steer dune development. *Front. Ecol. Evol.* **9**, 761336 (2021).
- Xie, D. et al. Mangrove removal exacerbates estuarine infilling through landscape-scale bio-morphodynamic feedbacks. *Nat. Commun.* **14**, 7310 (2023).
- van Der Heide, T. et al. Spatial self-organized patterning in seagrasses along a depth gradient of an intertidal ecosystem. *Ecology* **91**, 362–369 (2010).
- Barbier, E. B. et al. The value of estuarine and coastal ecosystem services. *Ecol. Monogr.* **81**, 169–193 (2011).
- Barbier, E. B. et al. The value of coastal wetland ecosystem services. In *Coastal Wetlands 2019*, 947–964 Elsevier (2019).
- Rietkerk, M. & Van de Koppel, J. Regular pattern formation in real ecosystems. *Trends Ecol. Evol.* **23**, 169–175 (2008).
- van de Koppel, J., Bouma, T. J. & Herman, P. M. The influence of local and landscape-scale processes on spatial self-organization in estuarine ecosystems. *J. Exp. Biol.* **215**, 962–967 (2012).
- De Paoli, H. et al. Behavioral self-organization underlies the resilience of a coastal ecosystem. *Proc. Natl. Acad. Sci.* **114**, 8035–8040 (2017).
- Xi, H., Dong, X., Chirayath, V., Gleason, A. C. & Purkis, S. J. Emergent coral reef patterning via spatial self-organization. *Coral Reefs* **44**, 273–289 (2025).
- Weerman, E. J. et al. Spatial self-organization on intertidal mudflats through biophysical stress divergence. *Am. Naturalist* **176**, E15–E32 (2010).
- Zhao, L. X., Xu, C., Ge, Z. M., Van De Koppel, J. & Liu, Q. X. The shaping role of self-organization: linking vegetation patterning, plant traits and ecosystem functioning. *Proc. R. Soc. B* **286**, 20182859 (2019).
- Manor, A. & Shnerb, N. M. Facilitation, competition, and vegetation patchiness: from scale free distribution to patterns. *J. Theor. Biol.* **253**, 838–842 (2008).
- Von Hardenberg, J., Kletter, A. Y., Yizhaq, H., Nathan, J. & Meron, E. Periodic versus scale-free patterns in dryland vegetation. *Proc. R. Soc. B: Biol. Sci.* **277**, 1771–1776 (2010).
- Siteur, K. et al. Phase-separation physics underlies new theory for the resilience of patchy ecosystems. *Proc. Natl. Acad. Sci.* **120**, e2202683120 (2023).
- Bouma, T. J. et al. Density-dependent linkage of scale-dependent feedbacks: a flume study on the intertidal macrophyte *Spartina anglica*. *Oikos* **118**, 260–268 (2009).
- Gittman, R. K. et al. Living on the edge: increasing patch size enhances the resilience and community development of a restored salt marsh. *Estuaries Coasts* **41**, 884–895 (2018).
- Wu, M. et al. Theory of scale-dependent feedback: An experimental validation and its significance for coastal saltmarsh restoration. *Sci. Total Environ.* **756**, 143855 (2021).
- Park, H. & Nepf, H. Turbulence in a channel with a patchy submerged canopy: the impact of spatial configuration. *J. Fluid Mech.* **1006**, A15 (2025).

26. Luijendijk, A. et al. The state of the world's beaches. *Sci. Rep.* **8**, 6641 (2018).
27. Baas, A. C. Chaos, fractals and self-organization in coastal geomorphology: simulating dune landscapes in vegetated environments. *Geomorphology* **48**, 309–328 (2002).
28. McGuiirk, M. T., Kennedy, D. M. & Konlechner, T. The role of vegetation in incipient dune and foredune development and morphology: a review. *J. Coast. Res.* **38**, 414–428 (2022).
29. Durán, O. & Moore, L. J. Vegetation controls on the maximum size of coastal dunes. *Proc. Natl. Acad. Sci. USA* **110**, 17217–17222 (2013).
30. Charbonneau, B. R. et al. Vegetation effects on coastal foredune initiation: wind tunnel experiments and field validation for three dune-building plants. *Geomorphology* **378**, 107594 (2021).
31. Reijers, V. C. et al. A Lévy expansion strategy optimizes early dune building by beach grasses. *Nat. Commun.* **10**, 2656 (2019).
32. Stauffer, D., & Aharony, A. *Introduction to percolation theory*. Taylor & Francis. (2018).
33. Mayaud, J. R. & Webb, N. P. Vegetation in drylands: effects on wind flow and aeolian sediment transport. *Land* **6**, 64 (2017).
34. Hesp, P. A., Dong, Y., Cheng, H. & Booth, J. L. Wind flow and sedimentation in artificial vegetation: field and wind tunnel experiments. *Geomorphology* **337**, 165–182 (2019).
35. Gross, B., & Havlin, S. *Percolation in Spatial Networks: Spatial Network Models Beyond Nearest Neighbours Structures*. Cambridge: Cambridge University Press. (2022).
36. Quintanilla, J. Measurement of the percolation threshold for fully penetrable disks of different radii. *Phys. Rev. E* **63**, 061108 (2001).
37. Hunt, A. G. & Sahimi, M. Flow, transport, and reaction in porous media: percolation scaling, critical-path analysis, and effective medium approximation. *Rev. Geophys.* **55**, 993–1078 (2017).
38. Kirkpatrick, S. Percolation and conduction. *Rev. Mod. Phys.* **45**, 574 (1973).
39. Keitt, T. H., Urban, D. L., & Milne, B. T. Detecting critical scales in fragmented landscapes. *Conservation ecology*, **1**, 4 (1997).
40. Duggan-Edwards, M. F., Pagès, J. F., Jenkins, S. R., Bouma, T. J. & Skov, M. W. External conditions drive optimal planting configurations for salt marsh restoration. *J. Appl. Ecol.* **57**, 619–629 (2020).
41. Schwarz, C. et al. Self-organization of a biogeomorphic landscape controlled by plant life-history traits. *Nat. Geosci.* **11**, 672–677 (2018).
42. Schwarz, C., van Rees, F., Xie, D., Kleinhans, M. G. & van Maanen, B. Salt marshes create more extensive channel networks than mangroves. *Nat. Commun.* **13**, 2022 (2017).
43. Bayraktarov, E. et al. The cost and feasibility of marine coastal restoration. *Ecol. Appl.* **26**, 1055–1074 (2016).
44. De Groot, R. S. et al. Benefits of investing in ecosystem restoration. *Conserv. Biol.* **27**, 1286–1293 (2013).
45. Silliman, B. R. et al. Harnessing ecological theory to enhance ecosystem restoration. *Curr. Biol.* **34**, R418–R434 (2024).
46. Morton, J. P. et al. Strategic planting and nutrient amendments to accelerate the revegetation of rapidly retreating coastal dunes. *J. Appl. Ecol.* **00**, 1–13 (2025).
47. Derijckere, J., Strypsteen, G. & Rauwoens, P. Early-stage development of an artificial dune with varying plant density and distribution. *Geomorphology* **437**, 108806 (2023).
48. Strypsteen, G., Bonte, D., Taelman, C., Derijckere, J. & Rauwoens, P. Three years of morphological dune development after planting marram grass on a beach. *Earth Surf. Process. Landf.* **49**, 2980–2997 (2024).
49. Silliman, B. R. et al. Facilitation shifts paradigms and can amplify coastal restoration efforts. *Proc. Natl. Acad. Sci.* **112**, 14295–14300 (2015).
50. Berghuis, P. M., Mayor, Á.G., Rietkerk, M. & Baudena, M. More is not necessarily better: The role of cover and spatial organization of resource sinks in the restoration of patchy drylands. *J. Arid Environ.* **183**, 104282 (2020).
51. He, Q. & Silliman, B. R. Climate change, human impacts, and coastal ecosystems in the Anthropocene. *Curr. Biol.* **29**, R1021–R1035 (2019).
52. Peterson, G., Allen, C. R. & Holling, C. S. Ecological resilience, biodiversity, and scale. *Ecosystems* **1**, 6–18 (1998).
53. Liu, Q. X. et al. Pattern formation at multiple spatial scales drives the resilience of mussel bed ecosystems. *Nat. Commun.* **5**, 5234 (2014).
54. Montreuil, A. L., Bullard, J. E., Chandler, J. H. & Millett, J. Decadal and seasonal development of embryo dunes on an accreting macrotidal beach: North Lincolnshire, UK. *Earth Surf. Process. Landf.* **38**, 1851–1868 (2013).
55. van Puijenbroek, M. E. et al. Embryo dune development drivers: beach morphology, growing season precipitation, and storms. *Earth Surf. Process. Landf.* **42**, 1733–1744 (2017a).
56. Silva, F. G., Wijnberg, K. M., de Groot, A. V. & Hulscher, S. J. The effects of beach width variability on coastal dune development at decadal scales. *Geomorphology* **329**, 58–69 (2019).
57. Broek, S. *The effects of storm surges on dune systems near inlets: A case-study for the Marsdiep inlet near Texel* (Master's thesis, University of Twente) (2017).
58. Nolet, C., Van Puijenbroek, M., Suomalainen, J., Limpens, J. & Riksen, M. UAV-imaging to model growth response of marram grass to sand burial: Implications for coastal dune development. *Aeolian Res.* **31**, 50–61 (2018).
59. Delgado-Fernandez, I. A review of the application of the fetch effect to modelling sand supply to coastal foredunes. *Aeolian Res.* **2**, 61–70 (2010).
60. van Puijenbroek, M. E. et al. Exploring the contributions of vegetation and dune size to early dune development using unmanned aerial vehicle (UAV) imaging. *Biogeosciences* **14**, 5533–5549 (2017b).
61. Lammers, C., Reijers, V. C. & van der Heide, T. Scale-dependent interactions in coastal biogeomorphic landscapes: Pioneer both inhibits and facilitates primary foredune builder across spatial scales. *Geomorphology* **467**, 109486 (2024).
62. Toms, J. D. & Lesperance, M. L. *Piecewise regression: a tool for identifying ecological thresholds*. *Ecology* **84**, 2034–2041 (2003).
63. Muggeo, V. M. Segmented: an R package to fit regression models with broken-line relationships. *R. N.* **8**, 20–25 (2008).
64. Bolker, B. M. et al. *Ecological Models And Data In R*. (Princeton University Press, 2008).

Acknowledgements

We thank the Waterschapshuis, Beeldmateriaal and the municipality of Texel for providing us with the aerial imagery, and Maarten Zwartz for his support in creating the digital elevation maps. Finally, we thank Willem-Jan Berghuis for his thoughtful contributions and valuable discussions during the analysis, and Ton Markus for improving the figures. This work is part of the Builders on the Beach project funded by the Netherlands Organization of Scientific Research (NWO, UUNIOZ_Builders on the beach 4543.1 awarded to TvdH and AGM). VCR was supported by NWO-Veni grant VI.Veni.212.059.

Author contributions

P.M.J.B. conceived the idea. T.v.d.H., M.R., V.C.R., J.v.d.K, A.G.M. and D.J.P.S. helped further conceptualizing the idea and provided input for the data analysis. P.M.J.B. designed the methodology and analyzed the data. P.M.J.B., T.v.d.H. and M.R. made an outline for the paper, P.M.J.B. wrote the original draft and all authors contributed to the subsequent drafts.

Competing interests

The authors declare no competing interests.

Additional information

Supplementary information The online version contains supplementary material available at <https://doi.org/10.1038/s41467-026-70552-7>.

Correspondence and requests for materials should be addressed to Paul M. J. Berghuis.

Peer review information *Nature Communications* thanks Dominic Robson, Orenco Duran Vinent, and the other, anonymous, reviewer for their contribution to the peer review of this work. A peer review file is available.

Reprints and permissions information is available at <http://www.nature.com/reprints>

Publisher's note Springer Nature remains neutral with regard to jurisdictional claims in published maps and institutional affiliations.

Open Access This article is licensed under a Creative Commons Attribution-NonCommercial-NoDerivatives 4.0 International License, which permits any non-commercial use, sharing, distribution and reproduction in any medium or format, as long as you give appropriate credit to the original author(s) and the source, provide a link to the Creative Commons licence, and indicate if you modified the licensed material. You do not have permission under this licence to share adapted material derived from this article or parts of it. The images or other third party material in this article are included in the article's Creative Commons licence, unless indicated otherwise in a credit line to the material. If material is not included in the article's Creative Commons licence and your intended use is not permitted by statutory regulation or exceeds the permitted use, you will need to obtain permission directly from the copyright holder. To view a copy of this licence, visit <http://creativecommons.org/licenses/by-nc-nd/4.0/>.

© The Author(s) 2026